Biomimics of [FeFe]-hydrogenases incorporating redox-active ligands

Orton, Georgia R.F.; Ringenberg, Mark R.; Hogarth, Graeme

DOI:
10.1016/j.jorganchem.2022.122472

Document Version
Publisher's PDF, also known as Version of record

Citation for published version (Harvard):
Orton, GRF, Ringenberg, MR & Hogarth, G 2022, 'Biomimics of [FeFe]-hydrogenases incorporating redox-active ligands: Ferrocene-bridged dithiolate complexes [$Fe_2(CO)_6(\mu\text{-}EC_5H_4FeC_5H_4E)$] (E = S, Se)', *Journal of Organometallic Chemistry*, vol. 978, 122472. https://doi.org/10.1016/j.jorganchem.2022.122472

Journal of Organometallic Chemistry 978 (2022) 122472

Contents lists available at ScienceDirect

Journal of Organometallic Chemistry

journal homepage: www.elsevier.com/locate/jorganchem

Biomimics of [FeFe]-hydrogenases incorporating redox-active ligands: Ferrocene-bridged dithiolate complexes $[Fe_2(CO)_6(\mu\text{-}EC_5H_4FeC_5H_4E)]$ (E = S, Se)

Georgia R.F. Orton[a], Mark R. Ringenberg[b,*], Graeme Hogarth[a,*]

[a] Department of Chemistry, King's College London, 7 Trinity Street, London SE1 1DB, United Kingdom
[b] Institut fur Anorganische Chemie, Universitat Stuttgart, Pfaffenwaldring 55, Stuttgart 70569, Germany

ARTICLE INFO

Article history:
Received 8 June 2022
Revised 29 July 2022
Accepted 7 August 2022
Available online 8 August 2022

Keywords:
[FeFe]-hydrogenase
Ferrocene-bridge
Dithiolate
Diiron
Redox-active
Biomimic
DFT

ABSTRACT

Ferrocene-bridged dithiolate complexes $[Fe_2(CO)_6(\mu\text{-}EC_5H_4FeC_5H_4E)]$ (E = S, Se) (**1-2**) have been studied as biomimics of [FeFe]-hydrogenases, ferrocene taking the role of an Fe_4S_4 surrogate. Both show a quasi-reversible electron reduction at $E_{1/2}$ = -1.81 V and -1.56 V respectively with IR SEC showing that it is Fe_2-based (ca. 50 cm^{-1} hypsochromic shift) and leads to a significant structural rearrangement with formation of a bridging carbonyl being at ca. 1715 cm^{-1}. They also show reversible one-electron oxidation with a small (ca. 15 cm^{-1}) hypsochromic ν(CO) shift, showing it is ferrocene-based, while oxidation of the Fe_2 centre occurs outside of the potential window. DFT calculations on **1** show that the HOMO is ferrocene-based, and the LUMO Fe_2-based, both in accord with the IR SEC results. However, the radical anion $[\mathbf{1}]^-$ is calculated to have an elongated metal-metal vector rather than a bridging carbonyl, although a complex with an open structure $[\mathbf{1}(\boldsymbol{\mu}\textbf{-CO})]^-$ in which one thiolate group moves from a bridging to a terminal position is energetically similar. For **2**, DFT shows the HOMO is Fe_2-based, which is not supported experimentally. Complexes **1-2** are proton-reduction catalysts at their first reduction potential in the presence of trifluoroacetic acid. DFT suggests two competing pathways for H_2 generation catalysed by **1**, occurring upon protonation of either $[\mathbf{1}]^-$ or $[\mathbf{1}(\boldsymbol{\mu}\textbf{-CO})]^-$ to give bridging and terminal hydride complexes respectively. For **2**, DFT suggests that $[\mathbf{2}(\boldsymbol{\mu}\textbf{-CO})]^-$ is only slightly higher in energy than $[\mathbf{2}]^-$, probably a result of the weaker Fe-Se vs Fe-S bond, and thus proton-reduction likely proceeds (primarily) through the open-structure isomer.

1. Introduction

The so-called H-cluster site of [FeFe]-hydrogenases (Fig. 1**a**) contains two redox sites, the diiron dithiolate centre and a ferredoxin linked to the former through a cysteine group [1], and strong coupling between the two is essential for its catalytic operation [2]. Over the past two decades, [FeFe]-ase biomimics have been extensively studied [3], but in the vast majority the focus has been on the redox and chemical properties of the Fe_2 centre, and models incorporating a second redox-active ligand remain relatively rare [4]. The first [FeFe]-ase biomimic to contain a second redox site was reported by Pickett and co-workers (L = 1,3,5-tris(4,6-dimethyl-3-mercaptophenylthio)-2,4,6-tris(*p*-tolyl-thio)benzene)) (Fig. 1**b**) [5] and subsequently a number of different approaches have been explored for the incorporation of a second redox site [4]. Ferrocene-containing Fe_4S_4 surrogates are attractive due to their accessibility and well-studied Fe(II)/Fe(III) redox couple, the latter being tunable via judicious choice of substituents. Examples include Rauchfuss's complex (Fig. 1**c**) [6] and the 1,1'-bis(diphenylphosphino)ferrocene (dppf) complex (Fig. 1**d**) [7]. In these and related complexes [8], the second redox group is connected via a phosphine moiety, the donor ability of which necessarily affects the redox potential of the Fe_2 centre. Alternative approaches have been explored, including attaching ferrocene onto the dithiolate bridge [9-11], for example, in this way one (Fig. 1**e**) [10] or more (Fig. 1**f**) [11] ferrocene sub-units can be incorporated and the reduction potential of the Fe_2 centre is barely altered [10]. A limitation of all these approaches is, however, the relatively long distance between the two redox centres and consequently their direct interaction, and likely impact on catalytic behavior, may be limited.

* Corresponding author.
E-mail address: graeme.hogarth@kcl.ac.uk (G. Hogarth).

https://doi.org/10.1016/j.jorganchem.2022.122472

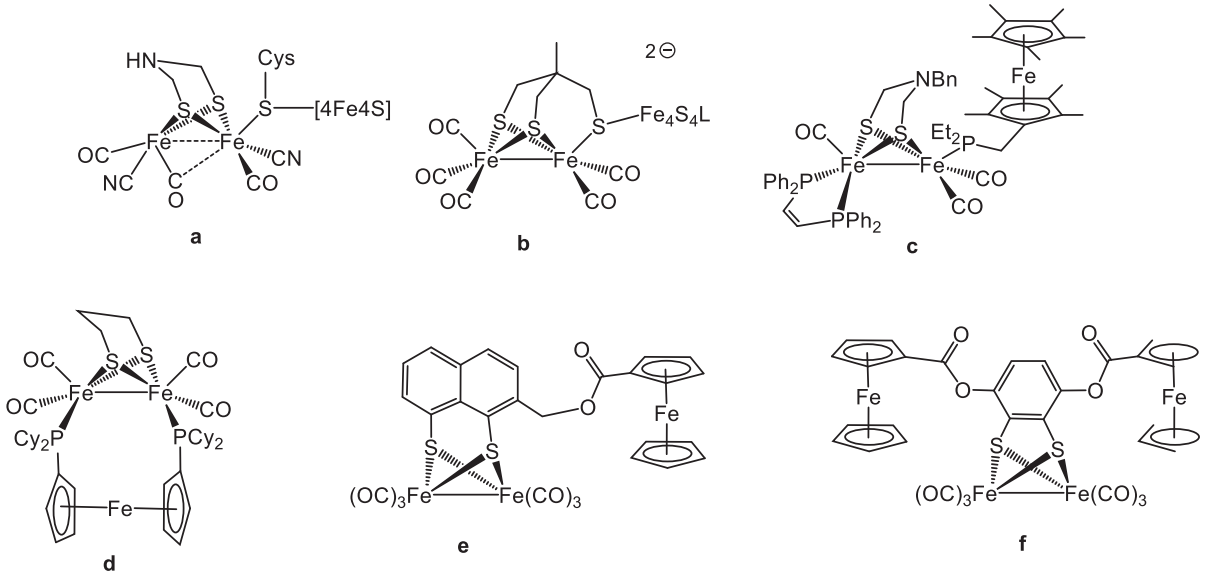

Fig. 1. Line drawings of (a) the active H-cluster site of [FeFe]-ases, (b)-(f) [FeFe]-ase biomimics containing at least two redox centres

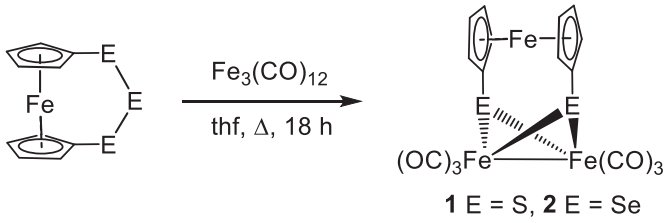

Scheme 1. Synthesis of ferrocene-containing **1-2**

An approach that ensures relatively close contact of the two redox centres is to incorporate ferrocene into the dithiolate backbone, as in $[Fe_2(CO)_6(\mu\text{-}EC_5H_4FeC_5H_4E)]$ (E = S, **1**; E = Se, **2**) (Scheme 1) [12-14]. Thus, in **1** the ferrocene centre sits only ca. 4.2 Å from the Fe_2 bond, and a low energy transition is observed at 590 nm in the UV-vis spectrum, being assigned to charge transfer from $Fe(C_5H_4S)_2$ to the diiron moiety [13]. One of us recently communicated the electrochemical properties and electrocatalytic proton-reduction behavior of **1** [13]. Herein, we develop this work, to include the selenium-analogue **2** and also investigate the oxidation chemistry of both.

2. Results and discussion

2.1. Synthesis and characterisation

Using a modified procedure, **1** was synthesised (Scheme 1**a**) by thermolysis of 1,2,3-trithia-[3]-ferrocene and $[Fe_3(CO)_{12}]$ for 18 h [13], with accompanying formation of $[Fe_3(\mu^3\text{-}S)_2(CO)_9]$. Selenium analogue **2** was prepared in a similar manner from 1,2,3-triselena-[3]-ferrocene, giving higher yields (48 %) than the previously documented photochemical synthesis (21%) [14]. Synthesis of **1-2** could also be carried out over shorter timeframes (ca. 4 h) in a microwave oven, albeit in lower yields.

IR spectra of **1-2** are characteristic of the $Fe_2(CO)_6(\mu\text{-}S)_2$ framework, the highest ν(CO) band for **2** at 2075 cm^{-1} being red shifted by ca. 6 cm^{-1} as compared to **1**, consistent with a small increase in electron density at the Fe_2 centre for the more electropositive chalcogen. ^{1}H NMR spectra of **1-2** are simple showing the symmetry of the ferrocene centre. Reaction times for the formation of **1-2** are significantly longer than for related closed bridgehead systems such as $[Fe_2(CO)_6(\mu\text{-bdt})]$ (bdt = 1,2-SC_6H_4S) [15,16]. Oxidative-addition of a thiol to $[Fe_3(CO)_{12}]$ initially results in formation of a thiolate-capped triiron cluster, the stability of which increases with increasing steric bulk and electron-donor properties of the thiolate [17,18]. Although no evidence for a persisting thiolate capped triiron cluster intermediate was observed by IR spectroscopy, it seems reasonable to suggest that increased stability of such a species with a bulky dichalocogeno-ferrocene may result in slow formation of the diiron dichalogenide species. Crystal structures of **1-2** have been previously been reported [13,14], the ferrocenyl moiety lying perpendicular to the Fe_2 bond, giving an overall C_{2v} symmetry. The presence of the larger chalcogen results in a slight elongation of the distance between the ferrocenyl iron and one Fe atom of the diiron bond from 4.2335 (5) Å in **1** to 4.4401 (6) Å in **2** [13,14]. In contrast, the diiron bond remains relatively unaffected at 2.5056 (4) in **1** and 2.5507 (5) in **2**.

2.2. Cyclic voltammetry (CV) and IR spectroelectrochemistry (IR SEC)

We studied the redox behaviour of 1-2 by cyclic voltammetry (CV) and IR spectroelectrochemistry (IR SEC), aspects of which were previously communicated for 1 [13]. A CV of 2 in CH_2Cl_2 is shown in Figure 2 and as might be expected, 1-2 show very similar redox behaviour. Each has a reversible oxidation at $E_{1/2}$ = + 0.14 V ($\Delta E = E_{pa}$ - E_{pc} = 110 mV) for 1 and $E_{1/2}$ = +0.37 V (ΔE 180 mV) for 2 (vs $[Fe(C_5H_5)_2]^{+/0}$ as internal reference) being largely independent of scan rate which, alongside its accessibility, suggests that it is ferrocene-based [19]. Both also have a quasi-reversible reduction at $E_{1/2}$ = -1.81 V (ΔE 220 mV) for 1 and $E_{1/2}$ = -1.56 V (ΔE 200 mV) for 2, and for the latter a further reduction at E_{pc} = -1.92 is also observed, in addition to a small oxidation wave at E_{pa} = -0.68 V associated with the reduction events. Oxidation of the Fe_2 centre likely occurs outside of the potential window provided by the solvent/electrolyte for both 1 and 2 [20].

We used IR SEC to further understand changes to **1-2** following oxidation and/or reduction. For both **1-2**, oxidation results in a hypsochromic shift of the ν(CO) bands, with the highest energy band shifting by ca. 15 cm^{-1} (Fig. 3**a**). This relatively small change confirms that oxidation localised at the ferrocene bridgehead. In contrast, reduction of **1-2** is localized at the diiron site, as evidenced by a ca. 50 cm^{-1} bathochromic shift of the ν(CO) bands due to increased back-bonding (Fig. 3**b**). The pattern changes

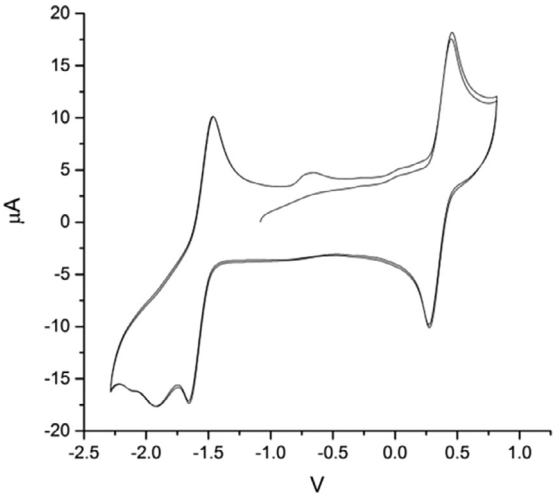

Fig. 2. CV of 2 (1 mM in 0.1 M Bu_4NPF_6/CH_2Cl_2 vs. $Fc^{+/0}$ at 0.1 Vs^{-1})

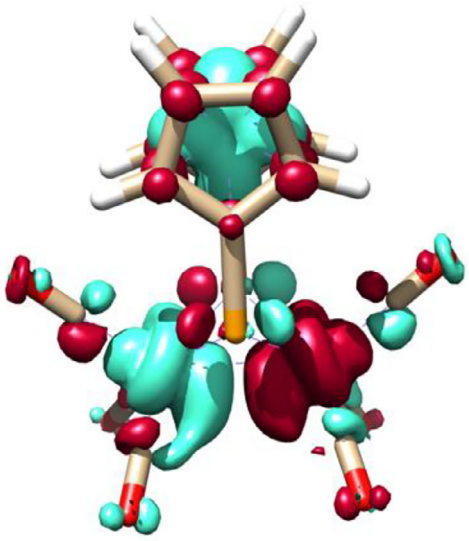

Fig. 4. Spin density of $\mathbf{2}^+$, isovalues = 0.002, spin up (teal), spin down (red).

slightly upon reduction, indicative of a geometric rearrangement, and a band at ca. 1715 cm^{-1} assigned to a bridging carbonyl confirms this [13].

2.3. DFT calculations

To better understand the nature of the one-electron oxidation and reduction events occurring in **1**-**2**, DFT calculations were carried out on both. The geometry-optimised model for **1** is in accord with the solid-state structure and shows that the HOMO is localised on the ferrocene and the LUMO on the diiron centre, being metal-metal anti-bonding in nature [13]. The former corroborates the SEC results, with the one-electron oxidation occurring at the ferrocene bridgehead. In contrast, despite the near identical spectroscopic behavior of the two, DFT calculations on **2** show that the HOMO is located at the Fe_2 centre (Fig. 4), although this conflicts with spectroscopic observations. This discrepancy is highlighted by the small observed hypsochromic shift of the ν(CO) shown in the IR SEC spectrum, which clearly shows that over the experimental timeframe oxidation is ferrocene-based, likely due to the ferrocene moiety being the kinetic site of oxidation.

Energies for the ferrocene HOMO and HOMO-1 located at **1** are -5.7356 eV and -5.7653 eV, respectively, while the HOMO-2 for the Fe_2S_2 core is -6.2393 eV. The increased electron density offered by the selenium to both the ferrocene bridgehead and the $Fe_2(CO)_6$ core inverts the location of the HOMO to be $Fe_2(CO)_6$ at -4.8823 eV, while the HOMO-1 and HOMO-2 are -5.3170 eV and -5.3453 eV. This energy inversion is not unexpected based on the increased electron density offered by the selenium donors, however, it is not evidently clear why the spectroscopic observations are nearly identical for **1** and **2**. The open-shell calculations helped to reveal a plausible explanation to the spectroscopic observations, finding a significant energy barrier between an electron hole located at the $Fe_2(CO)_6$ core and that located on ferrocene, such that the spin density is found across all three Fe sites. Open-shell calculations often overestimate the degree of electron delocalisation; however, the spectroscopic observations clearly point to ferrocene oxidation.

Unrestricted DFT calculations were carried out on the open-shell structure of $[\mathbf{1}]^-$ and show the added electron to be localised in the Fe_2 anti-bonding orbital, resulting in an elongation of the Fe-Fe vector [13], however, this structure does not have a bridging carbonyl (from IR SEC). Both $[Fe_2(CO)_6(\mu\text{-bdt})]$ [21] and $[Fe_2(CO)_6(\mu\text{-edt})]$ (edt = SCH_2CH_2S) [22], with rigid dithiolate bridges, undergo potential inversion and show a two-electron reduction with cleavage of an Fe-S bond and concomitant formation of a bridging carbonyl. On the basis of this, further DFT calculations

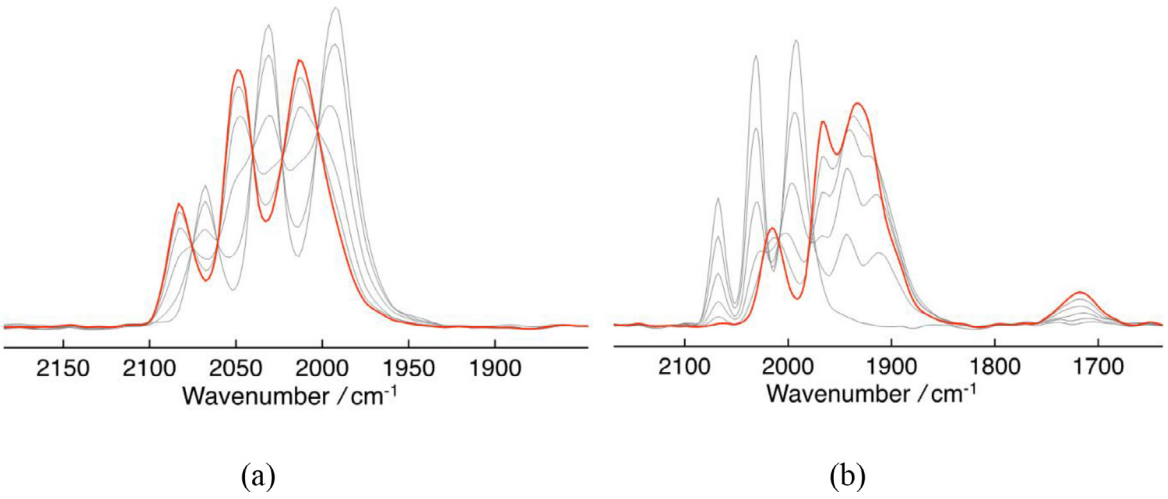

Fig. 3. IR spectra showing electrochemical conversion of **2** in CH_2Cl_2 to (a) oxidation product (red trace), (b) reduction product (red trace)

were run on a selection of open structures, and a second energy minimum identified, which is consistent with the spectroscopic information. From these calculations it was concluded that reduction of **1** induces isomerisation to an open structure $[\mathbf{1}]^{-*}$ in which one thiolate group moves from a bridging to a terminal position. The spin density of this structure is localised at one iron centre and one CO ligand from the Fe(0) centre moves into a semi-bridging position, pointing towards the Fe(I) centre. The open structure is further stabilised by a sulfur-based π-bond.

Based on calculations for the open structure of **1** [13], DFT analysis of **2** revealed a similar second energy minimum corresponding to a species, $[\mathbf{2}^{-}]^{*}$,with an open structure, a semi-bridging carbonyl and a Se-based π-bond (Fig. 5). This was expected since the spectrscopic data points towards the reduction of **1**-**2** resulting in formation of structurally similar complexes, anions $[\mathbf{1}(\boldsymbol{\mu}\text{-}\mathbf{CO})]^{-}$ and $[\mathbf{2}(\boldsymbol{\mu}\text{-}\mathbf{CO})]^{-}$ being structurally similar to $[Fe_2(CO)_6(\mu\text{-bdt})]^{2-}$[21], despite the latter being a two-electron reduction product. As previously mentioned, potential inversion upon reduction of $[Fe_2(CO)_6(\mu\text{-bdt})]$ results as the aromatic bdt ligand can stabilise the negative charge [21]. In contrast, reduction of **1**-**2** is a one-electron event, which may be attributed (in part) to the poor π-acceptor ability of cyclopentadienyl rings. For both $[\mathbf{1}\text{-}\mathbf{2}]^{-}$, whilst DFT predicts that formation of $[\mathbf{1}(\boldsymbol{\mu}\text{-}\mathbf{CO})]^{-}$ and $[\mathbf{2}(\boldsymbol{\mu}\text{-}\mathbf{CO})]^{-}$ is endothermic, experimentally we only observe open structures. The discrepancy may be due to limitations in the DFT model which gives gas-phase structures, and ignores the roles of solvent, counter ions and the electrode surface.

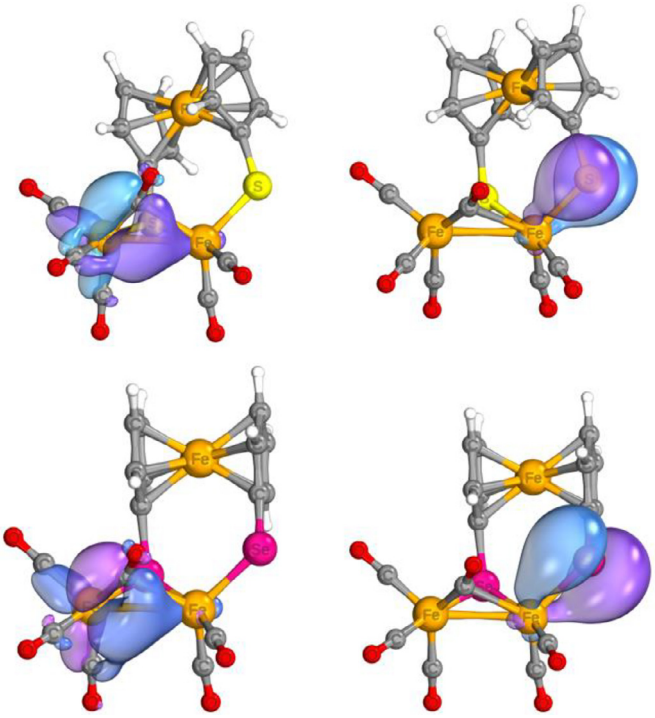

Fig. 5. Intrinsic bond orbital generated from open shell DFT calcualtions of $[1(\mu\text{-CO})]^{-}$ (top) and $[2(\mu\text{-CO})]^{-}$ (bottom) showing bridging CO bonding orbitals (left) and a π-orbital from the terminal chalcogenide (right)

3.3. Electrocatalytic proton-reduction

We previously reported [13] that (in MeCN) and with trifluoroacetic acid (TFA) as a proton source, **1** is an electrocatalyst for the hydrogen evolution reaction (HER). We have now tested **2** as an electrocatalyst for HER under analogous conditions (Fig. 6). Upon addition of TFA a new reduction wave appears at ca. -1.7 V corresponding to H_2 production [13]. The catalytic current grows

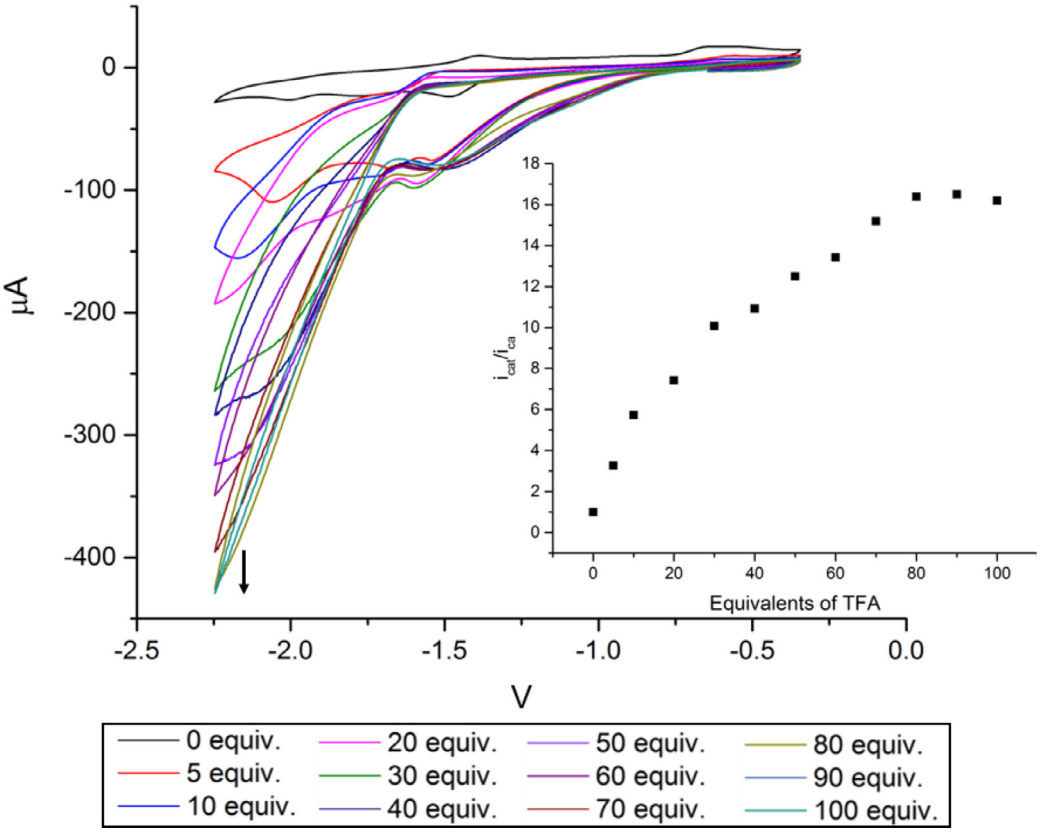

Fig. 6. CVs of 2 (1 mM in 0.1 M TBAFP/MeCN) in the presence of 0–100 equiv. of TFA; insert: plot of i_{cat}/i_{ca} (catalytic current / cathodic current) taken at -2 V.

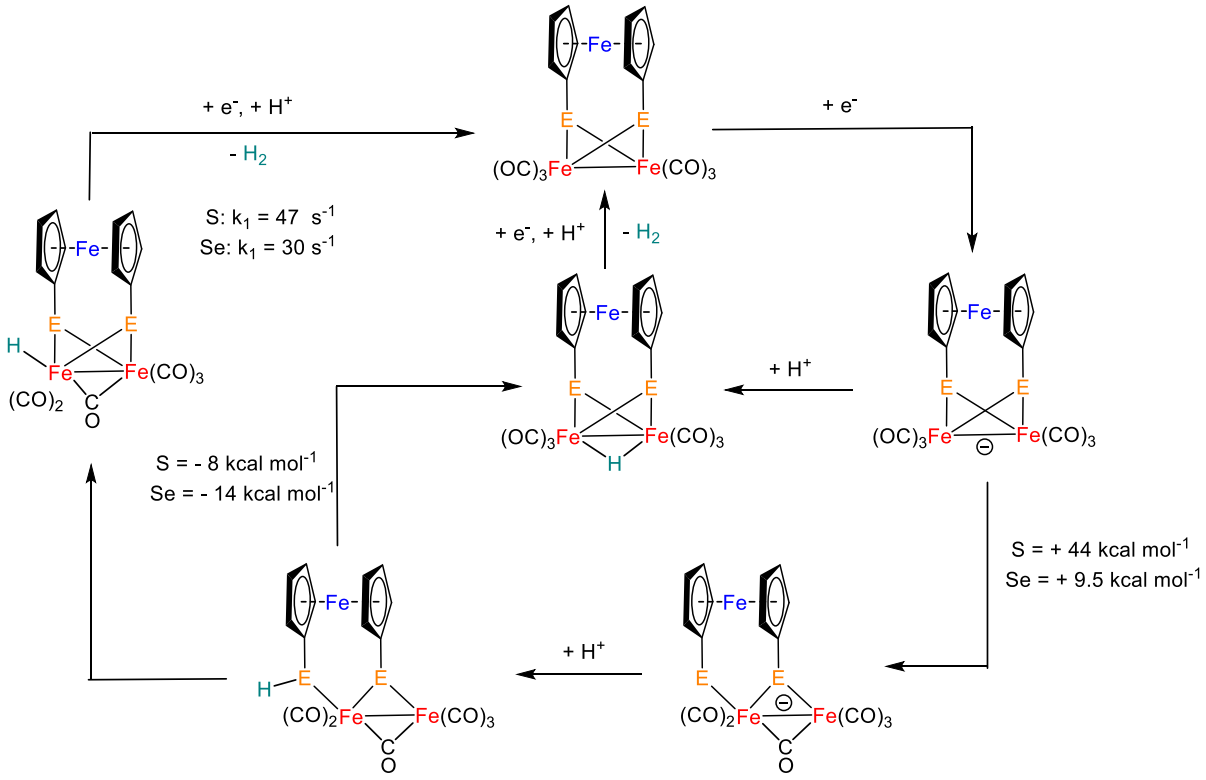

Fig. 7. DFT calculated proton-reduction pathways for 1-2

steadily upon addition of between 0–70 equivalents of acid, but the catalytic wave is less clearly defined than that seen with **1**. This possibly indicates that several HER processes occur simultaneously. From a plot of cathodic catalytic current (i_{cat}) against the cathodic current in the absence of acid (i_{ca}) it is evident that i_{cat} reaches a plateau after the addition of ca. 80 equivalents of acid, the rate of reaction becoming independent of acid concentration and steady state equilibrium has been achieved. It is likely, and consistent with studies of similar catalysts for proton-reduction, that the rate-limiting step is reductive elimination of H_2 [13]. Thus, the observed rate constant upon addition of 80 – 100 equivalents of acid corresponds to the rate of unimolecular H_2 elimination. A rate constant k_{cat} of 30 s^{-1} is calculated, representing the number of molecules of H_2 produced by each catalytic site per second, being slightly lower than that of 47 s^{-1} calculated for **1** under analogous conditions [13].

Based on DFT calculations, we previously suggested that two catalytic pathways operate for **1** [13]. The first pathway proceeds via reduction of **1** to [**1**]$^-$ which is followed by protonation to give a bridging hydride, while the second involves pre-formation of the open-complex [**1(*μ*-CO)**]$^-$, containing a terminal thiolate ligand and semi-bridging carbonyl. Protonation of the thiolate π-orbital followed by oxidative addition of the thiol generates a terminal hydride which are typically more active towards H_2 release [13].

In order to understand the difference in the rate constants between **1-2**, we returned to these DFT calculations. So-called, chalcogen slippage (Fig. 7) from [**2**]$^-$ to the open structure [**2(*μ*-CO)**]$^-$, which in turn permits access to a proton-reduction pathway involving a terminal hydride, is calculated to be significantly less endothermic than the same process for **1**. This suggests that **2** is more able to support an open structure upon reduction, thus facilitating access to a proton-reduction pathway involving a terminal hydride and might therefore be expected to exhibit superior HER activity. However, while protonation of [**1(*μ*-CO)**]$^-$ to give a terminal hydride is favored over formation of a bridging hydride, the two routes have similar energies for [**2(*μ*-CO)**]$^-$. This would reduce catalyst efficiency and may explain the lower activity of **2** over **1** in the presence of TFA. In some cases, strong acids, such as HBF_4 have been shown to favor formation of terminal hydrides over bridging hydrides [23]. Consequently, **2** was tested as an electrocatalyst (in MeCN) using HBF_4 as a proton source. Unfortunately, addition of sequential equivalents of HBF_4 resulted in large negative currents which did not appear to follow any trend. IR spectroscopy showed that addition of HBF_4 to a degassed CH_2Cl_2 solution of **2** (see **Fig. S1**) results in oxidation of the ferrocene centre to give [**2**]$^+$, likely explaining the unusual currents observed by CV. The instability of the reduced form of **3** precluded its testing as a proton reduction catalyst. Its accessible oxidation chemistry prompted us to probe H_2 oxidation activity by NMR spectroscopy, however no evidence of any reaction with H_2 was found.

3. Summary and conclusions

In this contribution we have significantly developed the biomimic chemistry of [$Fe_2(CO)_6(\mu$-$EC_5H_4FeC_5H_4E)$] (**1-2**) [13], containing two redox centres held in closely proximity. For both, reduction is Fe_2 based and oxidation if ferrocene-based as clearly shown by IR SEC. This view is largely supported by DFT studies, although for **2** it is not in full accord suggesting that oxidation should be Fe_2-based. Both **1-2** reduce protons (TFA in MeCN) at their first reduction potential with **1** being marginally more efficient. DFT studies suggest that two competing pathways operate, differing in the structure of the reduced monoanions, which can have all terminal or a single bridging carbonyl ligand. Unfortunately, the inaccessible oxidation of the Fe_2 centre has negated attempts to oxidise H_2 and we have recently sought to address this by phosphine-substitution, studies which will be reported in due course.

4. Experimental

4.1. General

All reactions were carried out using standard Schlenk-line techniques under N_2 using anhydrous solvents. Work-up was carried out in air using standard bench reagents. NMR spectra were recorded on a BrukerAvance 400 MHz Ultrashield NMR spectrometer and referenced internally to residual solvent peaks or externally to $P(OMe)_3$ ($^{31}P\{^1H\}$). High resolution electron spray ionisation mass spectra were recorded on a Bruker Daltronics Esquire 3000 spectrometer at Imperial College, London. FTIR spectra were recorded on a IRAffinity-1S Shimadzu spectrophotometer in a solution cell fitted with calcium fluoride plates, subtraction of the solvent absorptions being achieved by computation.

4.2. CV and IR SEC

Electrochemistry was carried out in anhydrous degassed MeCN or CH_2Cl_2 solutions using 0.1 M $[Bu_4N][PF_6]$ as the supporting electrolyte. An Autolab Interface 6 potentiostat was used for electrochemical measurements. Unless otherwise stated, the working electrode was a 3 mm diameter glassy carbon electrode that was polished with diamond slurry. The counter electrode was a Pt wire and the quasi-reference electrode was a silver wire or Pt electrode. All CVs were referenced to the $Fc^{+/0}$ or $Fc^{*+/0}$ redox couples. Proton reduction studies were carried out by adding equivalents of $HBF_4.Et_2O$ (Sigma-Aldrich) which was used as supplied. IR SEC spectra were obtained using a Nicolet 6700 FT-IR instrument using an OTTLE cell equipped with a CaF_2 window.

4.3. Computational methodology

DFT calculations [24] were carried out using the ORCA program package [25]. Structures were calculated using the molecular structures of **1-2** as a base. The structures of the anions and cations were calculated from the optimised structures of the neutral species with additional electron(s). Geometry optimisations were carried out at the B3LYP level of DFT [25,26].

4.4. Synthesis

4.4.1. $[Fe_2(CO)_6(\mu\text{-}SC_5H_4FeC_5H_4S)]$ (1)

$[Fe_3(CO)_{12}]$ (2.07 g, 4.1 mmol) and 1,2,3-trithia[3]ferrocenophane (1.00 g, 3.57 mmol) were combined in dry, degassed THF and stirred under reflux for 18 h. The solution was cooled to room temperature, filtered through celite with CH_2Cl_2 (20 ml), and the solvent was removed under reduced pressure. The product was purified on a 30 cm long silica gel column (hexanes). The first fraction was deep purple $[Fe_3(\mu^3\text{-}S)_2(CO)_9]$. The second brown band gave **1** (603 mg, 32 %) as a dark brown solid after removal of solvents under reduced pressure. ^1H NMR ($CDCl_3$) δ 4.33 (s, 4H Cp), 4.01 (s, 4H, Cp); IR (CH_2Cl_2) ν(CO): 2075s, 2039vs, 2004s, 1996w cm^{-1}. Characterisation was consistent with previously published data [13].

4.4.2. $[Fe_2(CO)_6(\mu\text{-}SeC_5H_4FeC_5H_4Se)]$ (2)

$[Fe_3(CO)_{12}]$ (1.37 g, 2.73 mmol) and 1,2,3-triselena[3]ferrocenophane (1.00 g, 2.38 mmol) were combined in dry, degassed THF and stirred under reflux for 18 h. The solution was cooled to room temperature, filtered through celite with CH_2Cl_2 (20 ml), and the solvent was removed under reduced pressure. The product was purified on a 30 cm long silica gel column (hexanes). The first fraction was deep purple $[Fe_3(\mu^3\text{-}Se)_2(CO)_9]$. The second brown band gave **2** (710 mg, 48 %) as a dark brown solid after removal of solvent under reduced pressure ^1H NMR ($CDCl_3$) δ 4.32 (t, J = 1.8 Hz, 4H, Cp), 4.13 (t, J = 1.8 Hz, 4H, Cp). IR (CH_2Cl_2) ν(CO): 2069s, 2032vs, 1992s cm^{-1}. Characterisation is consistent with previously published data [14].

Declaration of Competing Interest

The authors declare no competing interest.

Data availability

The authors do not have permission to share data.

Acknowledgements

We thank King's College London for the provision of a PhD studentship (GRFO) and Dr Caroline Knapp (UCL) for advice regarding the synthesis of 1,2,3-trithia-[3]-ferrocene.

Supplementary materials

Supplementary material associated with this article can be found, in the online version, at doi:10.1016/j.jorganchem.2022.122472.

References

[1] Y. Nicolet, C. Piras, P. Legrand, C.E. Hatchikian, J.C. Fontecilla-Camps, Struct. 7 (1999) 13–23; J.W. Peters, W.N. Lanzilotta, B. Lemon, L.C. Seefeldt, Science 282 (1988) 1853–1858; B.J. Lemon, J.W. Peters, Biochemistry 38 (1999) 12969–12973; Y. Nicolet, A.L. De Lacy, X. Vernéde, V.M. Fernandez, E.C. Hatchikian, J.C. Fontecilla-Camps, J. Am. Chem. Soc. 123 (2001) 1596–1601.
[2] C. Sommer, A. Adamska-Venkatesh, K. Pawlak, J.A. Birrell, O. Rüdiger, E.J. Reijerse, W. Lubitz, J. Am. Chem. Soc. 129 (2017) 1440–1443; F. Wittkamp, M. Senger, S.T. Stripp, U.-P. Apfel, Chem. Commun. 54 (2018) 5934–5942; V.S. Thoi, Y. Sun, J.R. Long, C.J. Chang, Chem. Soc. Rev. 42 (2013) 2388–2400.
[3] For reviews of this area see;; I.P. Georgakaki, L.M. Thomson, E.J. Lyon, M.B. Hall, M.Y. Darensbourg, Coord. Chem. Rev. 238-239 (2003) 255–266; D.J. Evans, C.J. Pickett, Chem. Soc. Rev. 32 (2003) 268–287; T.B. Rauchfuss, Inorg. Chem. 43 (2004) 14–26; L. Sun, B. Åkermark, S. Ott, Coord. Chem. Rev. 249 (2005) 1653–1663; X. Liu, S.K. Ibrahim, C. Tard, C.J. Pickett, Coord. Chem. Rev. 249 (2005) 1641–1652; C. Tard, C.J. Pickett, Chem. Rev. 109 (2009) 2245–2274; J.-F. Capon, F. Gloaguen, P. Schollhammer, J. Talarmin, Coord. Chem. Rev. 249 (2005) 1664–1676; J.-F. Capon, F. Gloaguen, F.Y. Pétillon, P. Schollhammer, J. Talarmin, Eur. J. Inorg. Chem. (2008) 4671–4681; D. Schilter, J.M. Camara, M.T. Huynh, S. Hammes-Schiffer, T.B. Rauchfuss, Chem. Rev. 116 (2016) 8693–8749; D. Schilter, J.M. Camara, M.T. Huynh, S. Hammes-Schiffer, T.B. Rauchfuss, Chem. Rev. 116 (2016) 8693–8749; F. Wittkamp, M. Senger, S.T. Stripp, U.-P. Apfel, Chem. Commun. 54 (2018) 5934–5942; F. Arrigoni, L. Bertini, R. Breglia, C. Greco, L. De Gioia, G. Zampella, New J. Chem. 44 (2020) 17596–17615; J.T. Kleinhaus, F. Wittkamp, S. Yadav, D. Siegmund, U.-P. Apfel, Chem. Soc. Rev. 50 (2021) 1668–1784.
[4] Y.-C.C. Liu, T.-H.H. Yen, K.-T.T. Chu, M.-H. Chiang, Comments Inorg. Chem. 36 (2015) 141–181.
[5] C. Tard, X. Liu, S.K. Ibrahim, M. Bruschi, L. De Gioia, S.C. Davies, X. Yang, L.-S. Wang, G. Sawers, C.J. Pickett, Nature 433 (2005) 610–613.
[6] J.M. Camara, T.B. Rauchfuss, Nat. Chem. 4 (2012) 26–30; J.C. Lansing, J.M. Camara, D.E. Gray, T.B. Rauchfuss, Organometallics 33 (2014) 5897–5906.
[7] S. Ghosh, G. Hogarth, N. Hollingsworth, K.B. Holt, S.E. Kabir, B.E. Sanchez, Chem. Commun. 50 (2014) 945–947; G.R.F. Orton, S. Ghosh, L. Alker, J.C. Sarker, D. Pugh, M.G. Richmond, F. Hartl, G. Hogarth, Dalton Trans 51 (2022) 9748–9769.
[8] Y. Si, K. Charreteur, J.-F. Capon, F. Gloaguen, F.Y. Pétillon, P. Schollhammer, J. Talarmin, J. Inorg. Biochem. 104 (2010) 1038–1042; R. Becker, S. Amirjalayer, P. Li, S. Woutersen, J.N.H. Reek, Sci. Adv. 2 (2016) e1501014; S. Ghosh, N. Hollingsworth, M. Warren, D.A. Hrovat, M.G. Richmond, G. Hogarth, Dalton Trans 48 (2019) 6051–6060.
[9] X. de Hatten, E. Bothe, K. Merz, I. Huc, N. Metzler-Nolte, Eur. J. Inorg. Chem. (2008) 4530–4537; X. Zeng, Z. Li, Z. Xiao, Y. Wang, X. Liu, Electrochem. Commun. 12 (2010) 342–345.
[10] J. Zhao, Z. Wei, X. Zeng, X. Liu, Dalton Trans. 41 (2012) 11125-11133.
[11] G. Qian, W. Zhong, Z. Wei, H. Wang, Z. Xiao, L. Long, X. Liu, New J. Chem. 39 (2015) 9752–9760; G. Qian, H. Wang, W. Zhong, X. Liu, Electrochim. Acta 163 (2015) 190–195.
[12] D. Seyferth, B.W. Hames, Inorg. Chim. Acta 77 (1983) L1–L2.
[13] M. Häßner, J. Fiedler, M.R. Ringenberg, Inorg. Chem. 58 (2019) 1742–1745.
[14] P. Mathur, A. Raghuvanshi, S.M. Mobin, J. Organomet. Chem. 794 (2015) 266–273.
[15] G.A.N. Felton, A.K. Vannucci, J. Chen, L.T. Lockett, N. Okumura, B.J. Petro, U.I. Zakai, D.H. Evans, R.S. Glass, D.L. Lichtenberger, J. Am. Chem. Soc. 129 (2007) 12521–12530.

[16] J.A. Cabeza, M.A. Martínez-García, V. Riera, D. Ardura, S. García-Granda, Organometallics 17 (1998) 1471–1477.
[17] J.A. De Beer, R.J. Haines, J. Organomet. Chem. 24 (1970) 757–767.
[18] S. Ghosh, S. Basak-Modi, M.G. Richmond, E. Nordlander, G. Hogarth, Inorg. Chim. Acta 480 (2018) 47–53.
[19] D. Astruc, Eur. J. Inorg. Chem. 2017 (2017) 6–29.
[20] R.J. Day, A.J. Gross, E.S. Donovan, K.D. Fillo, G.S. Nichol, G.A.N. Felton, Polyhedron 197 (2021) 115043.
[21] G.A.N. Felton, A.K. Vannucci, J. Chen, L.T. Lockett, N. Okumura, B.J. Petro, U.I. Zakai, D.H. Evans, R.S. Glass, D.L. Lichtenberger, J. Am. Chem. Soc. 129 (2007) 12521–12530.
[22] J.F. Capon, F. Gloaguen, P. Schollhammer, J. Talarmin, J. Electroanal. Chem. 595 (2006) 47–52.
[23] F. Gloaguen, T.B. Rauchfuss, Chem. Soc. Rev. 38 (2009) 100–108; D. Schilter, J.M. Camara, M.T. Huynh, S. Hammes-Schiffer, T.B. Rauchfuss, Chem. Rev. 116 (2016) 8693–8749.
[24] M.J. Frisch, G.W. Trucks, H.B. Schlegel, G.E. Scuseria, M.A. Robb, J.R. Cheeseman, G. Scalmani, V. Barone, B. Mennucci, G.A. Petersson, H. Nakatsuji, M. Caricato, X. Li, H.P. Hratchian, A.F. Izmaylov, J. Bloino, G. Zheng, J.L. Sonnenberg, M. Hada, M. Ehara, K. Toyota, R. Fukuda, J. Hasegawa, M. Ishida, T. Nakajima, Y. Honda, O. Kitao, H. Nakai, T. Vreven, J.A. Montgomery, J.E. Peralta, F. Ogliaro, M. Bearpark, J.J. Heyd, E. Brothers, K.N. Kudin, V.N. Staroverov, R. Kobayashi, J. Normand, K. Raghavachari, A. Rendell, J.C. Burant, S.S. Iyengar, J. Tomasi, M. Cossi, N. Rega, J.M. Millam, M. Klene, J.E. Knox, J.B. Cross, V. Bakken, C. Adamo, J. Jaramillo, R. Gomperts, R.E. Stratmann, O. Yazyev, A.J. Austin, R. Cammi, C. Pomelli, J.W. Ochterski, R.L. Martin, K. Morokuma, V.G. Zakrzewski, G.A. Voth, P. Salvador, J.J. Dannenberg, S. Dapprich, A.D. Daniels, J.B. Farkas, J.V. Foresman, J. Ortiz, D.J. Cioslowski, Fox, Gaussian 09, Revis. B.01, Gaussian, Inc., Wallingford CT, 2009.
[25] A.D. Becke, J. Chem. Phys. 98 (1993) 5648–5652.
[26] P.J. Stephens, F.J. Devlin, C.F. Chablowski, M.J. Frisch, J. Phys. Chem. 98 (1994) 11623–11627.